Hindawi
Journal of Nanomaterials
Volume 2019, Article ID 4146190, 14 pages
https://doi.org/10.1155/2019/4146190

Research Article

Structure and Biological Properties of Surface-Engineered Carbon Nanofibers

Wojciech Smolka,[1] Agnieszka Panek,[2] Maciej Gubernat,[3] Aneta Szczypta-Fraczek,[3] Piotr Jelen,[3] Czeslawa Paluszkiewicz,[2] Jaroslaw Markowski,[1] and Marta Blazewicz[3]

[1]*Laryngology Department, School of Medicine in Katowice, Medical University of Silesia in Katowice, Poland*
[2]*Institute of Nuclear Physics, Polish Academy of Sciences, Krakow, Poland*
[3]*AGH University of Science and Technology, Faculty of Materials Science and Ceramics, Krakow, Poland*

Correspondence should be addressed to Marta Blazewicz; mblazew@agh.edu.pl

Received 30 January 2019; Revised 1 April 2019; Accepted 9 April 2019; Published 9 May 2019

Academic Editor: Enrico Bergamaschi

The aim of this work was to manufacture, using the electrospinning technique, polyacrylonitrile- (PAN-) based carbon nanofibers in the form of mats for biomedical applications. Carbon nanofibers obtained by carbonization of the PAN nanofibers to 1000°C (electrospun carbon nanofibers (ECNF)) were additionally oxidized in air at 800°C under reduced pressure (electrospun carbon nanofibers oxidized under reduced pressure (ECNFV)). The oxidative treatment led to partial removal of a structurally less-ordered carbon phase from the near-surface region of the carbon nanofibers. Both types of carbon fibrous mats were studied using scanning electron microscopy (SEM), high-resolution transmission electron microscopy (TEM), XRD, and Raman spectroscopy. The morphology, microstructure, and surface properties of both materials were analyzed. The oxidative treatment of carbon nanofibers significantly changed their surface morphology and physical properties (wettability, surface electrical resistance). Biological tests (genotoxicity, fibroblast, and human osteoblast-like MG63 cultures) were carried out in contact with both materials. Genotoxicity study conducted by means of comet assays revealed significant differences between both carbon nanofibers. Fibroblasts contacted with the as-received carbon nanofibers (ECNF) showed a significantly higher level of DNA damage compared to control and oxidized carbon nanofibers (ECNFV). The ECNFV nanofibers were not cytotoxic, whereas ECNF nanofibers contacted with both types of cells indicated a cytotoxic effect. The ECNFV introduced into cell culture did not affect the repair processes in the cells contacting them.

1. Introduction

Modern medicine applies more and more therapeutic solutions based on the achievements of nanotechnology and nanomaterials. Materials with reduced dimensions to nanoscale, i.e., nanomaterials, are often characterized by specific physical and chemical properties, which are of particular interest in terms of potential medical applications [1]. Research on new forms of nanomaterials has resulted in the development of a number of new solutions in the field of medical therapies and diagnostics, including biosensors, implantable electrodes, materials for drug carriers and anticancer therapy, and development of new methods for tissue engineering and regenerative medicine [2–4]. The development of regenerative medicine and tissue engineering is to a large extent related to the achievements of nanotechnology [5–7]. Tissue engineering is an area that is based on biomimetic scaffolds modified with bioactive agents. Cells colonizing the tissue scaffold have desirable conditions for proliferation and differentiation. It is well known that endogenous electric fields play an important role in controlling cellular functions, such as morphology, gene expression, proliferation, and migration. Research is being conducted on the development of alternative cellular activation processes, and electrical stimulation is one of the directions of research in nerve engineering, as well as in the treatment of cardiac and skeletal muscles [8–15]. It was shown that introducing electric field stimulation in cell-based treatment is a

beneficial physical factor affecting the effectiveness of tissue engineering methods. Such tissue supports are attractive solutions for the needs in stem cell therapy. Interactions between stem cells and their environment *in vivo* conditions are very complex involving biochemical factors, extracellular matrix components, and physical factors affecting cell behavior. All these elements, used to regulate processes in stem cells, are very important factors creating favorable conditions in stem cell therapy [16–21].

Otolaryngology, like cardiac surgery or neurosurgery, is looking for new solutions in the field of therapy methods using electric conductive nanomaterials for the construction of both implantable electrodes and nanomaterials allowing the construction of substrates for tissue engineering and stem cell therapy. Hearing loss is a common human disease caused by irreversible damage to hair cells and spiral ganglion neurons in the mammalian cochlea. There are many therapeutic solutions to treat this disease, such as hearing aids and cochlear implants, that can provide good retrieval of the hearing function [22–24]. Research is being carried out on the development of a biological method to repair a damaged cochlea that can restore normal hearing without any implant materials or hearing aid devices. These kinds of premises have become the driving force to develop stem cell therapy in otolaryngology [25–28].

Carbon nanoforms, such as nanotubes, graphene, or carbon nanofibers, have proven to be materials with high potential in the development of new implants and medical devices [29–31]. Due to their electron properties, high electrical conductivity, biomimetic form, and unique surface properties, they can be used in the construction of implantable electrodes and biosensors and as the tissue substrates for *in vitro* and *in vivo* applications. For this reason, electric field stimulation, thanks to conductive properties of the carbon substrates, may become a method regulating, both *in vivo* and *in vitro*, the cells' behavior.

However, all the carbon nanoforms can interact with tissues and cells exhibiting a toxic effect. Recent works on the biocompatibility of CNT have proved a significant influence of the way they were prepared for contact with cells and tissues [30–34]. Many studies indicated that the critical parameters determining biological behavior of CNT are the surface morphology, chemical surface state, and their homogeneous dispersion in the biological system [35–37]. The functionalization of CNT proved their solubility and altered cellular interaction pathways, resulting in a significant reduction of cytotoxic effects [32, 38–40]. The presence of carboxyl or hydroxyl groups also resulted in the reduction of agglomerates and in the increase of the degree of dispersion, which inhibited the phenomenon called frustrated phagocytosis, in which the proteolytic enzymes and toxic substances were released from the cells, negatively affecting the biocompatibility of the CNT. On the other hand, there are also reports on cytotoxic effects of functionalized nanotubes and their genotoxic effect [41, 42].

Graphene also finds applications in medicine including materials for biosensors for early detection of cancer and cancer cell imaging/mapping, in targeted drug delivery systems, and in gene therapy [43–47].

Another group of carbon nanomaterials are carbon nanofibers produced by the controlled heat treatment of nanometric polymer precursors. This nanomaterial significantly differs in the structure and microstructure from CNT, has a larger diameter, and is generally characterized by a lower degree of structural ordering [48–50]. Carbon nanofibers due to their nanometric fibrous nature and physical properties, including electrical conductivity, have become particularly interesting as potential electrode biosensors, as material for the design of electrically conductive tissue substrates, and also as biomimetic forms that can be easily functionalized, depending on destination.

Our earlier study has shown that this form of carbon also requires a specific treatment to remove toxic carbonaceous fractions that may appear in its structure and that can be responsible for its biological behavior [51]. To date, many works have been devoted to the biocompatibility of CNT and graphene, while much less works have been published on the biocompatibility of carbon nanofibers.

The aim of this work is to present a new approach to manufacture biocompatible carbon nanofibers that can find applications in medicine for the construction of implants and medical devices as biosensors, microelectrodes, and electrical conductive scaffolds.

The study compares the genotoxicity and cytotoxicity of carbon nanofibers obtained from the electrospun PAN fiber precursor, differing in final chemical treatment, while retaining similar conditions of heat treatment during carbonization.

2. Materials and Methods

Copolymer Mavilon Zoltek Company (Hungary) consisting of 93–94 wt% of acrylonitrile mers, 5–6 wt% of methyl acrylate mers, and approximately 1 wt% of sodium alilosulfonate mers was used to manufacture polymer nanofibers. The polyacrylonitrile (PAN) nanofibers were spun from the polymer solution using the electrospinning method. The details of the PAN-based nanofiber precursor are described elsewhere [52]. The conversion of PAN nanofibers into carbon nanofibers consisted of three steps. The first step was the stabilization, during which the polymer nanofibers were oxidized in air up to about 300°C. The stabilized nanofibers were then carbonized by heating them in a nitrogen atmosphere to 1000°C at a heating rate of 5°C/min, without holding the samples at final temperature. Subsequently, carbon nanofibers were polythermally annealed from room temperature (RT) to 800°C in the air at the heating rate of 20°C/min, under reduced pressure of 0.1 atm. The parameters of the oxidation process were optimized to prevent possible combustion of the nanofibers. This step is aimed at modifying the near-surface region of carbon nanofibers in an oxidizing atmosphere. During this process, carbon fiber mats lost about 8% of the initial mass.

The following types of carbon nanofibers were prepared for further study: the as-received carbon nanofibers denoted as ECNF (electrospun carbon nanofibers) and carbon nanofibers after oxidation under reduced pressure in the air denoted as ECNFV.

To characterize the morphology of the carbon nanofibers and their surface, a scanning electron microscope (SEM; Nova Nanos 200, FEI COMPANY EUROPE) was used. SEM microphotographs and image analysis software (ImageJ 1.50b) were used to determine the nanofiber diameters as an average diameter of 30 measurements and the porosity of samples in the form of mats. The surface chemical properties were estimated using water contact angle (θ) measurements (DSA10; Kruss, Germany) enabling to evaluate the wettability of the carbon mats. Deionized water used in the experiments was prepared in PURELAB UHQ apparatus, ELGA LabWater (USA).

Electrical resistance measurements of the carbon nanofiber mats were conducted using a two contact probe (Metex multimeter, model M-3660D). The changes in the resistance of the samples in the temperature range from -190°C to +50°C, in the air atmosphere, were registered. Two copper wire electrodes were fixed on the surface samples (5×10 mm surface area) with a silver glue. Due to the form of the samples, i.e., very thin mats, the surface resistivity per square was determined.

A FEI Tecnai TF20 X-TWIN high-resolution transmission electron microscope was used to examine the microstructural features of carbon samples.

The Raman spectroscopy measurements were made using a Renishaw inVia Raman microspectrometer in the reflection mode with 50x objective magnifications using 442 nm and 514.5 nm laser lines as the excitation sources. The spectra were obtained with 5% of the laser beam power and with exposure time equal to 10 s. The spectra were collected from the sample with ca. 1-3 mW of the laser beam power. Each sample was analyzed in four different areas to obtain averaged results. The spectra obtained in the range of 100–3200 cm^{-1} with an argon laser wavelength 514.5 nm were analyzed using Fityk 0.8.0 software [53].

The deconvolution of the spectra was made using the Pseudo-Voigt function. Deconvolution allowed distinguishing the characteristic bands of the carbon structure. The parameters characterizing the carbon samples, i.e., R_1 and L_a, were determined. The R_1 parameter describes the degree of carbon crystallinity. This parameter was determined from the formula $R_1 = I_{D1}/I_G$, where I is the area under the analyzed D1 (disordered carbon phase) and G (ordered carbon phase) bands of the Raman spectrum [54].

L_a describes the crystallite size in the a-axis direction (along the graphene layers) of the polycrystalline carbon nanofiber structure. This parameter was determined from the Cancado equation, i.e., $L_a = (2.4 \times 10 - 10)\lambda_l^4 (I_{D1}/I_G)^{-1}$, where λ_l is the laser wavelength [54, 55].

An X-ray diffraction (XRD) study was carried out using an X'Pert Pro Philips X-ray diffractometer. The measurements were made using a copper radiation source lamp (CuKα1, $\lambda = 0.154056$ nm). Using the Scherrer formula, $L_c = k\lambda/(B\cos\theta)$, and the Bragg formula, $n\lambda = 2d\sin\theta$, the apparent crystallite sizes and the c-axis spacing, d_{002}, were determined. B is the half width at peak maximum (rad), θ is the Bragg angle (in rad), and k is the Scherrer constant taken as 1. The software, OriginPro 8.0 and Fityk 0.9.8, was used to deconvolute the (002) profiles of carbon samples. The line shapes of profiles were fitted using Gaussian and Lorentzian functions.

Table 1: Characterization of carbon nanofiber mats.

Sample	Nanofiber diameter (nm)	Material porosity (%)	Wettability θ (°)	Electrical conductivity (kΩ/square)
ECNF	301 ± 54	82.3 ± 9.4	113.3 ± 1.0	2.21
ECNFV	291 ± 68	86.6 ± 12.7	86.2 ± 0.9	3.69

Infrared (FT-IR) spectra were recorded using a Bio-Rad FTS 165 spectrometer, with a resolution of 2 cm^{-1}, within the range of 4000–400 cm^{-1}.

To determine potential genotoxicity of carbon nanofibers (ECNF, ECNFV), the normal human skin fibroblasts from cell line CCL-110 (American Type Culture Collection (ATCC)) were used. The cells were cultured in MEM medium at 37°C and 5% CO_2. The crumbled carbon mats (7.5 mg/4 ml PBS, phosphate-buffered saline) were mixed by means of an ultrasonic probe (Palmer Instruments) for 2 min. Sample's suspension (500 μl) was added to a well containing cells in 2 ml culture medium. Fibroblasts were contacted with nanomaterials at 37°C for 1 h or 24 h; next, the cells were washed in PBS and analyzed by comet assay procedure. The choice of 1-hour incubation resulted from time needed to enter the nanoparticles into the cell and possible interaction with DNA. Observation of DNA damage level after a 24-hour incubation with nanofibers allowed obtaining information on the durability of the effects of interaction with DNA and the impact on the integrity of DNA strands (apoptosis-related DNA fragmentation). The analysis of DNA damage levels after *in vitro* treatment was performed using the alkaline version of the comet assay [56, 57].

In addition, two experiments were carried out, in which cell cultures containing both types of nanofibers were exposed to radiation—1 Gy for 1 h and 24 h. In normal cells irradiated with the 1 Gy dose, the damage caused by radiation should be repaired within 24 hours of incubation. Comparison of T-DNA values in such planned experiments, in addition to data related to genotoxicity and cytotoxicity, may provide information on the destruction of repair processes in cells contacted with carbon nanofibers.

The suspension of *in vitro* treated fibroblasts was embedded in agarose on microscope slides. The cells and nuclear membranes were then lysed for 1 h in the agarose by detergent (1% Triton X-100) in alkaline pH > 13. Next, the DNA was subjected to alkaline electrophoresis (30 min, 4°C, 30 V, and 300 mA). After ethidium bromide (17 mg/ml) staining of cells, cellular DNA was visualized using the epifluorescence microscope Olympus BX-50 (Olympus, Tokyo, Japan). For the analysis of the comet pictures, the Komet 3.0 program from Kinetic Imaging Company (Liverpool, UK) was used. DNA damage was quantified by the T-DNA-tail DNA (DNA percentage in the comet tail), where the changes in the distribution of tail DNA are considered as a sensitive indicator of initial DNA breakage and DNA repair. Additionally, for all samples the number of dead cells per 100 cells

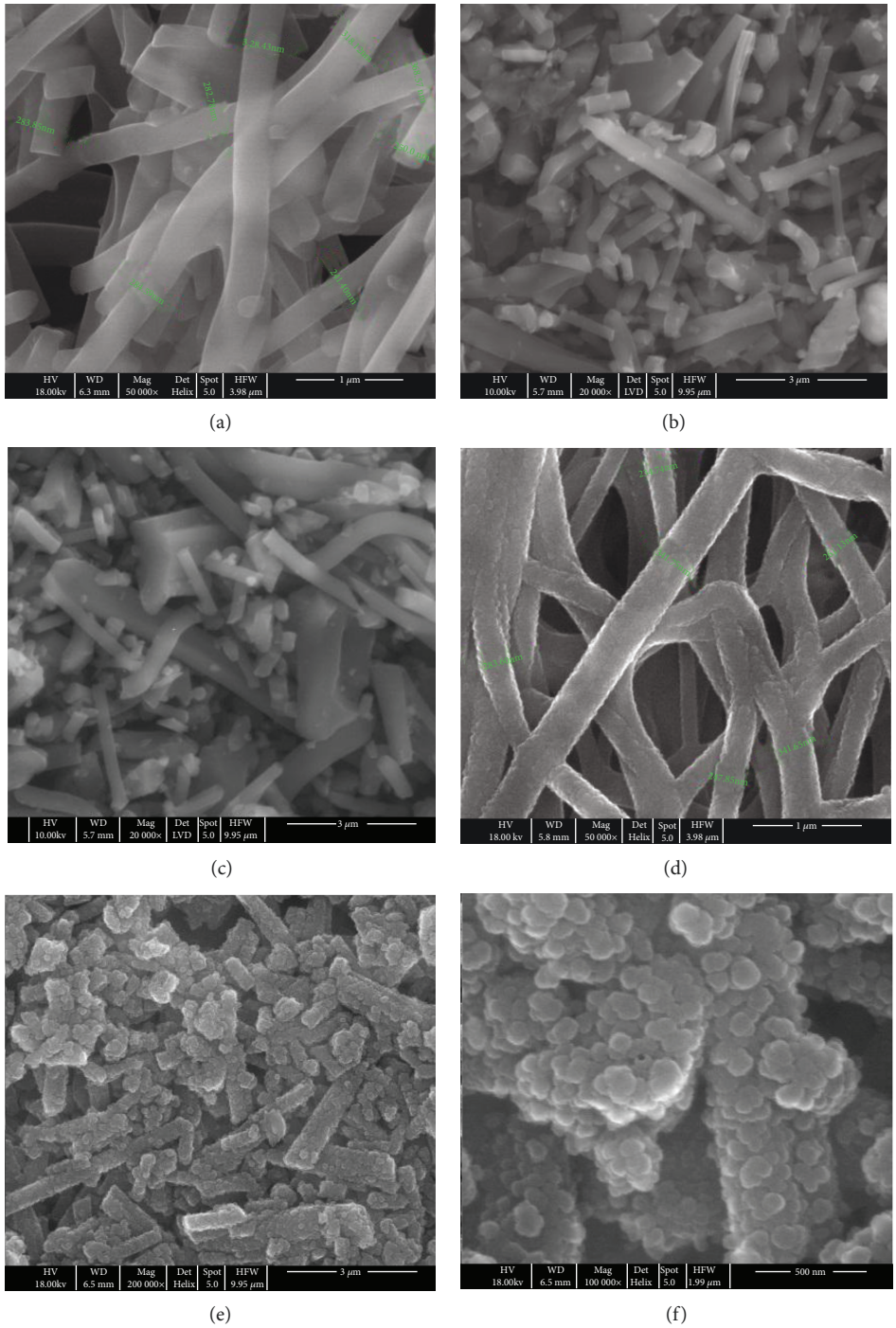

Figure 1: SEM microphotographs of carbon nanofibers: (a) ECNF, (b, c) ECNF after fragmentation, (d) ECNFV, and (e, f) ECNFV after fragmentation.

was counted. Two independent experimental replicates were performed for each aliquot: 200 cells were analyzed for each data point (2 slides per dose, 100 cells analyzed from each slide).

The data were presented as mean values and standard error. The statistical analysis was performed using the Student t test from Excel software. The p values equal to or less than 0.05 were considered significant. For the biological tests, material samples were sterilized by UV-C light.

In order to assess the morphology and viability of the human osteoblast-like MG63 cells (European Collection of Cell Cultures, Salisbury, UK) cultured on two types of nanofibers, live cell imaging employing a double staining of cells with cell-permeable calcein AM (marker of viable cells) and propidium iodide (marker of dead cells) dyes was performed. The fragmented carbon mats (7.5 mg/4 ml PBS) were mixed by means of an ultrasonic probe (Palmer Instruments) for 2 min. Sample's suspension (500 μl) was added to a well

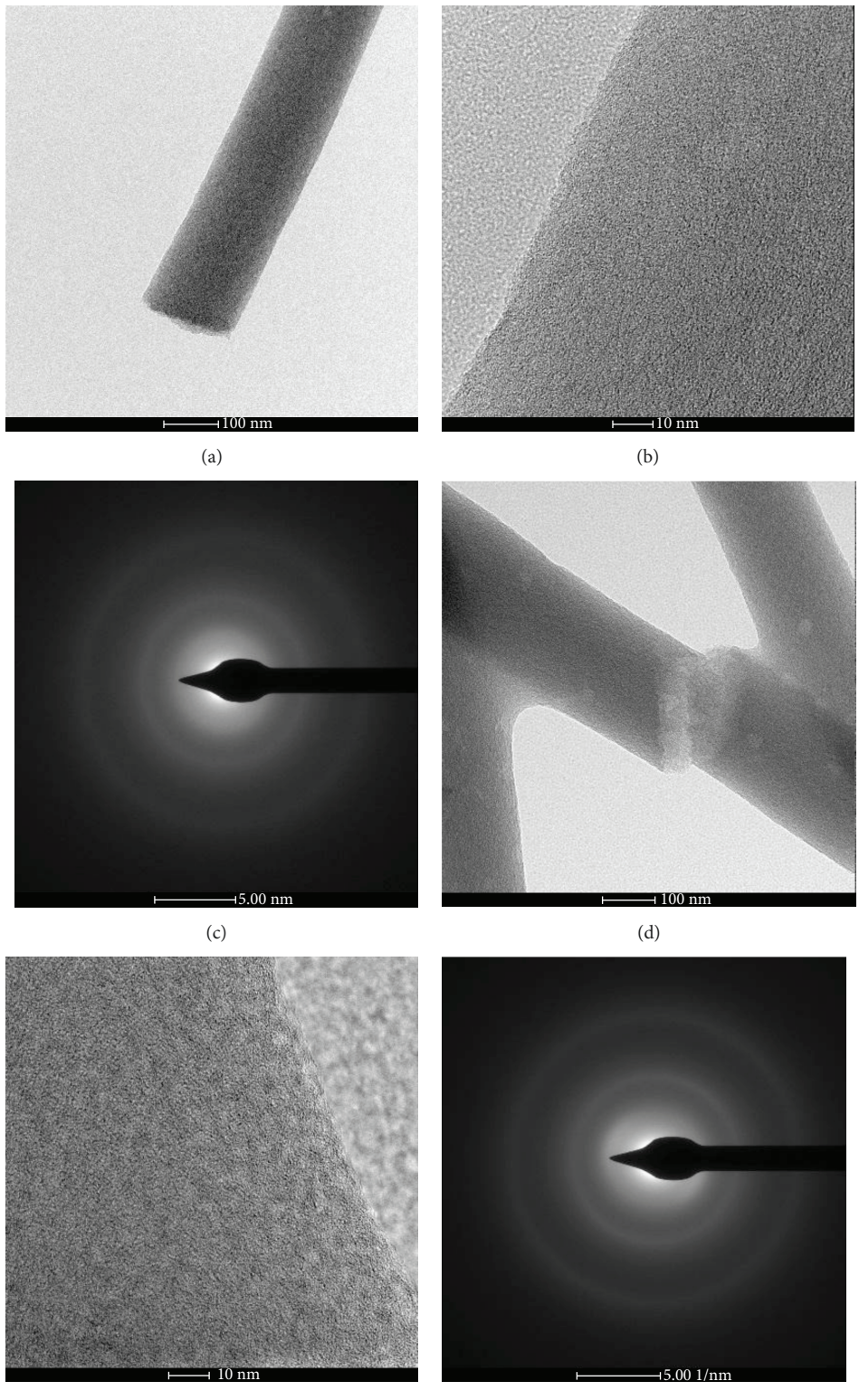

Figure 2: High-resolution TEM images of carbon nanofibers: (a) ECNF, (b) longitudinal section of ECNF, (c) selected-area electron diffraction patterns (SAED) of ECNF, (d) ECNFV, (e) longitudinal section of ECNFV, and (f) ECNFV-SAED.

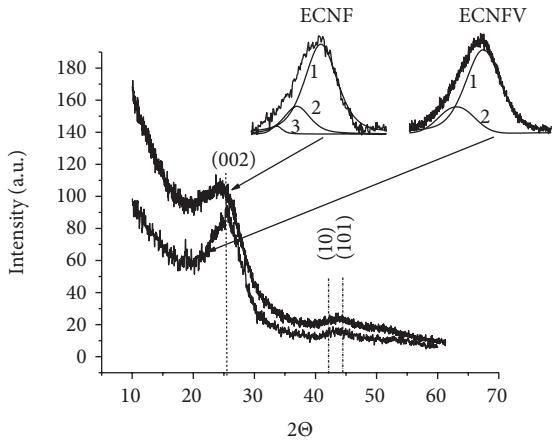

Figure 3: XRD patterns of carbon nanofibers and deconvoluted (002) peak of ECNF into three bands and ECNFV into two bands.

containing cells in 2 ml culture medium (Dulbecco's modified Eagle's minimum essential medium (Sigma) supplemented with 10% fetal bovine serum (Sebak GmbH, Germany) and gentamicin (40 μg/ml, LEK, Slovenia)) at 37°C in a humidified air atmosphere containing 5% of CO_2. The prepared samples were observed under a fluorescence microscope (Zeiss Axiovert 40, Carl Zeiss, Germany).

3. Results and Discussion

3.1. Characterization of Carbon Nanofiber Mats. Parameters characterizing the surface properties and microstructure of carbon samples in the form of mats are presented in Table 1. Water contact angle measurements were performed in order to evaluate the chemical nature of the materials' surfaces. The calculated θ value for ECNF was 113,3°, which is characteristic for hydrophobic materials. The ECNFV samples exhibit a distinctly smaller value (86,2°), indicating a more hydrophilic character of the nanofibers' surface caused by the oxidative treatment.

An average thickness of carbon mats was in the range of 40-60 μm with an average porosity of 82%±6%. The average diameter of single nanofibers in the ECNF mats was 301 nm. As can be seen from this table, the porosity of the carbon mats increased as a result of oxidation, and the diameter of a single nanofiber decreases. The physical properties of the mat, i.e., the wettability and surface resistance, also change.

SEM microphotographs of both types of carbon nanofibers are shown in Figure 1.

As can be seen from the microphotographs, both types of nanofibers are clearly different. The surface of the ECNF is smooth, and their diameter is uniform along their length. In our experiments, the carbon nanofibers were oxidized under polythermal conditions, i.e., from the RT to 800°C. The nanofibers consist of small crystallites connected by intercrystallite boundaries (see further XRD and Raman spectroscopy studies). Such a structure of the nanofibers makes the boundaries lower resistant to oxidation, and the images of the surface topography of these nanofibers after oxidation are a consequence of their diversified microstructure (Figure 1(d)). Images of both types of disintegrated nanofibers also distinctly differ; the ECNF particles (Figures 1(b) and 1(c)) have sharp edges, they are larger compared to the ECNFV particles (Figures 1(e) and 1(f)), and their cross-section surfaces are typical as for brittle materials. The particles formed from ECNFV are characterized by rounded edges, and they are distinctly smaller.

High-resolution TEM images of both types of carbon nanofibers are shown in Figure 2.

The images show the longitudinal sections of ECNF (b) and ECNFV (e), as well as their selected-area electron diffraction patterns (SAED). The ECNF nanofibers represent homogeneous turbostratic carbon crystallites, randomly distributed along the nanofiber length (Figure 2(b)). Three nanofibers subjected to air oxidation (ECNFV) show a greater microstructural heterogeneity; regions of the well-ordered crystallites and less ordered areas can be seen. Selected area electron diffraction (SAED) was performed on both carbon nanofibers, and the images for ECNF and ECNFV are shown in Figures 2(c) and 2(f), respectively. Both patterns are similar showing the diffraction rings consisting of continuous lines, which confirms a polycrystalline nature of these nanofibers.

The X-ray diffraction patterns of carbon samples with deconvolution of (002) peaks are shown in Figure 3.

The diffractograms show single broad and weak peaks at 23-26° 2θ, which correspond to (002) crystallographic planes. The shape and intensities of these peaks indicate that the microstructure of the nanofibers is strongly diversified. The diffractograms also show weak and broad peaks in the angular range of $2\theta \approx 42 - 45°$, corresponding to (10) and (101) planes.

The microstructural parameter, L_c, and the interplanar distance between graphene planes, d_{002}, determined from the diffraction patterns of carbon mats are collected in Table 2.

The (002) peaks after deconvolution indicate that the ECNF sample consists of three carbon phases, and the ECNFV sample contains two carbon phases differing in structural ordering (Figure 3). The dominant carbon phase 1 in both samples, due to the largest 2θ values, represents the carbon phase with a better structural ordering (Table 2). The carbon crystallites have a relatively high interplanar graphene distance d_{002} values, typically observed in turbostratic PAN-derived carbon fiber and nanofibers [52]. Carbon nanofiber after additional oxidation is composed of crystallites with a slightly better structural ordering, as evidenced by the lack of carbon phase 3 and a slight shift of the maximum of the deconvoluted (002) peak (1) towards higher 2θ values, i.e., from 25.272° for ECNF to 25.403° for ECNFV. The crystallites size, L_c, of carbon phase 1 in the ECNFV is higher, and at the same time the interlayer spacing, d_{002}, in these crystallites is smaller (0.350 nm) compared to ECNF (0.352 nm). Based on the ratio of the surface area of the (002) peaks after deconvolution to the total surface area of the (002) peak, the fractions of carbon phases were determined. The fraction of the carbon phase 1, representing the highest structural ordering in the ECNFV, is slightly higher

Table 2: Crystallographic data of carbon phases determined from X-ray diffractograms.

	ECNF			ECNFV	
	Carbon phase 1	Carbon phase 2	Carbon phase 3	Carbon phase 1	Carbon phase 2
2θ (°)	25.272	21,725	18.692	25.403	21.635
d_{002} (nm)	0.352	0.409	0.474	0.350	0.410
L_c (nm)	1.48	1.84	4.33	1.44	1.50
Carbon phase fraction (%)	78.31	19.34	2.35	82.2	17.8

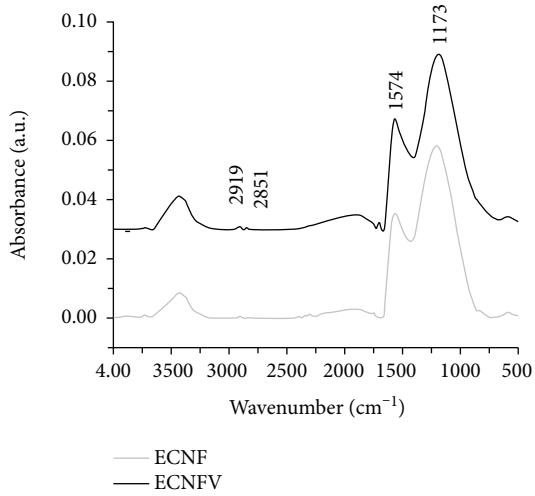

Figure 4: FTIR spectra of carbon nanofibers.

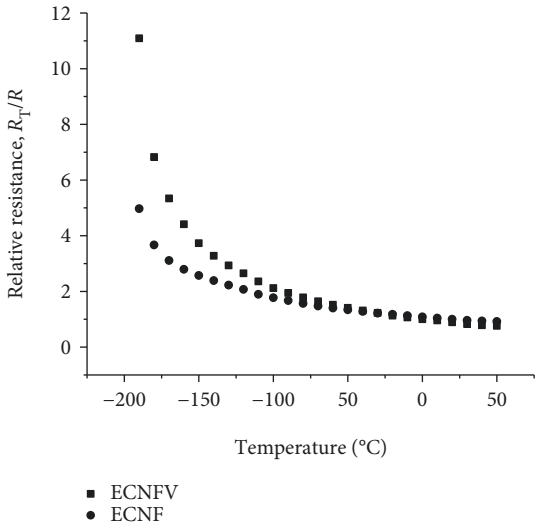

Figure 5: Relative resistance changes of carbon nanofibers in function of temperature.

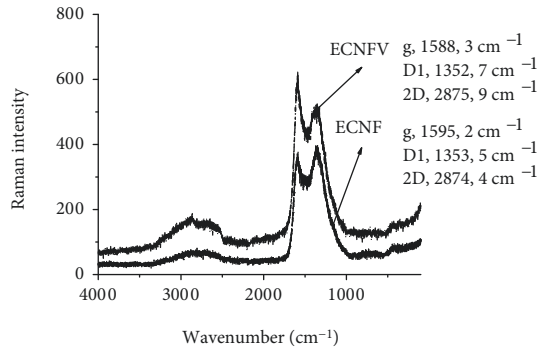

Figure 6: Raman spectra of carbon nanofibers.

(82.2%) as compared to ECNF (78.31%), which may indicate that during the oxidation a selective process of carbon removal with a lower structural ordering takes place.

The XRD analysis confirms a turbostratic structure of carbon nanofibers composed of small crystallites connected by intercrystallite boundaries containing also other carbon elements, i.e., hydrogen, nitrogen, and oxygen. Such intercrystallite phases are characterized by a less ordered structure than crystallites. It can therefore be expected that the carbon phases with a less-ordered structure, such as those forming the boundaries between crystallites in the carbon nanofibers, are more prone to the oxidation than a better organized carbon structure, e.g., the crystallites.

FTIR spectra of both nanofibers in Figure 4 show no difference in characteristic bands.

The as-received carbon nanofibers (ECNF) are characterized by low degree of structural ordering, typical for turbostratic structure of carbon materials [52].

The spectrum of the as-received carbon nanofibers contains broad overlapping bands between 950 cm^{-1} and 1600 cm^{-1}, coinciding with the band at 1574 cm^{-1} attributed to C=C vibration bonds of the graphene rings. The broad band is brought about by the presence of the single bonds between carbon and oxygen, hydrogen, and nitrogen. Carbon nanofibers were obtained from the electrospun PAN nanofiber precursor. Due to the stabilization process of the PAN nanofibers which took place in the air atmosphere, carbon nanofibers heat-treated at 1000°C contain some amount of oxygen, nitrogen, and hydrogen. Nitrogen and hydrogen in the carbon nanofiber structure are a residue of the PAN nanofiber precursor, while oxygen, in a small amount, is a consequence of the stabilization process of the PAN nanofibers. Both spectra contain weak bands at 2851 cm^{-1} and 2919 cm^{-1}, which correspond to the stretching vibrations of the C-H groups. The aromatic and aliphatic CH groups are usually found in the low-carbonized PAN-based carbon fibers (to 1000°C). The presence of hydrogen is also confirmed by the analysis of the Raman spectra described in the further part of the work. The spectrum of the oxidized nanofibers indicates that such a treatment, involving the removal of amorphous carbon, results in the formation of

Table 3: Parameters determined from deconvoluted Raman spectra of ECNF and ECNFV.

Sample	D1 band position (cm^{-1})	G band position (cm^{-1})	D3 band position (cm^{-1})	D4 band position (cm^{-1})	2D band position (cm^{-1})	L_a (nm)	R_1
ECNF	1353.5	1595.2	1516.8	1129.8	2786.4	4.4	4.28
ECNFV	1352.7	1588.3	1511.1	1125.6	2875.9	7.1	2.69

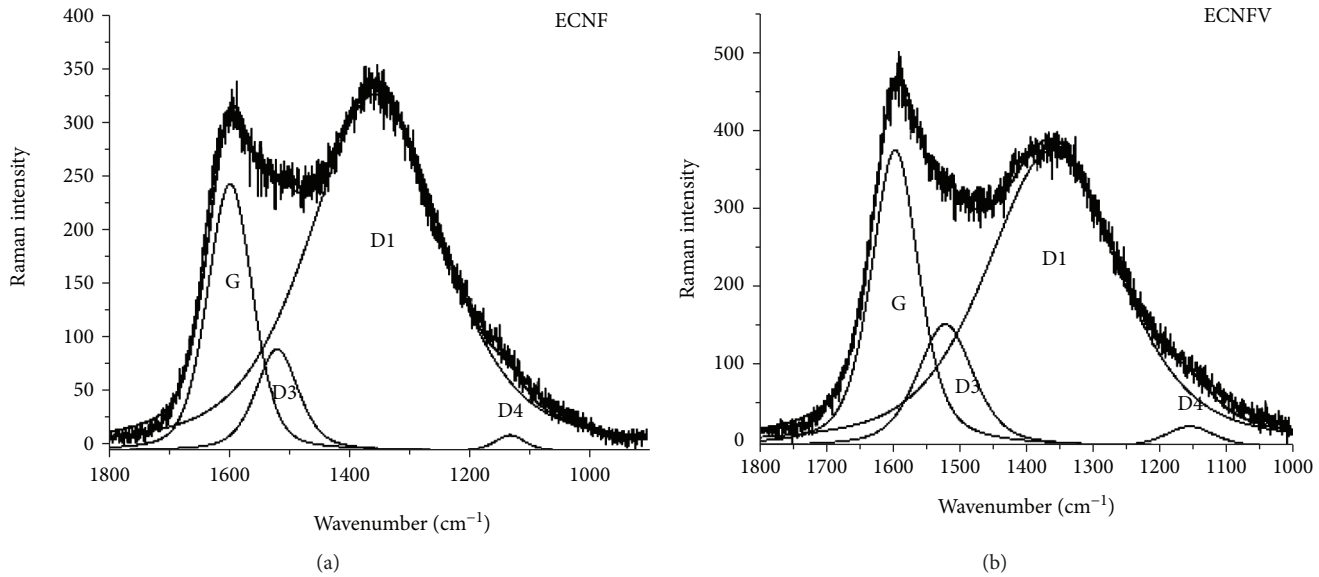

Figure 7: Deconvoluted Raman spectra of the first-order bands of two types of nanofibers.

gaseous products and does not lead to the formation of additional chemical groups with oxygen on the nanofiber surface, as is the case of the oxidation of carbon nanofibers with liquid oxidants [38]. The presence of nitrogen is due to the C-N bonds in the heterocyclic structure in PAN-derived carbon nanofibers carbonized at 1000°C.

Changes in the resistance of carbon samples as a function of temperature are shown in Figure 5.

For both samples, the curves showing the resistance changes are similar; i.e., with the temperature increase, the resistance decreases; this is behavior of materials characterized by semiconductor-like properties. A higher RT surface resistivity (Ro = 3.69 kΩ/sq) displays carbon samples after oxidative treatment compared to the as-received carbon nanofibers (2.21 kΩ/sq). The higher surface resistance of the carbon mat is a consequence of the change in its surface morphology as a result of oxidation. As SEM pictures show (Figure 1), the treatment removes a fraction of the carbon forming conductive pathways, mainly from the boundaries between the carbon crystallites. Such a process may lead to the formation of the surface fiber defects. For this reason, the slope of the curve for the ECNFV at lower temperatures is greater compared to ECNF.

Further differences in the structure of both types of carbon nanofibers were obtained by analysis of the Raman spectra shown in Figure 6. Table 3 summarizes the Raman spectra analysis and contains values of wavenumbers for G and D bands and L_a parameters determined after deconvolution of the first order bands.

Raman spectra reveal distinct differences in the structure of both nanofibers. The intensity ratio, R_1, of D to G bands, giving information about the degree of disordered and ordered phases in a carbon sample, indicates that the treatment distinctly enhances the fraction of the ordered carbon phase in nanofibers. Deconvolution made for the first-order bands of Raman spectra is shown in Figure 7.

The spectrum of ECNF contains peaks related to differently ordered carbon phases centered at 1129.8 cm^{-1} (D4 band), 1353.5 cm^{-1} (D1 band), and 1595.2 cm^{-1} (G band). The poorly organized carbon materials show also band at 1516.8 cm^{-1} (D3) assigned to defects outside the aromatic layers [58]. The spectrum in Figure 5 also contains peak centered at 2786 cm^{-1} (2G band) associated with the second order of the D band of the carbon phase. The G-band peak at 1592.5 cm^{-1} attributed to the radial C-C stretching mode of sp^2 bonded carbon is characteristic for a well-ordered carbon structure [59]. The D1 band of the carbon nanostructure can be attributed to the disordered carbon phase. The I_D/I_G peak intensity ratio is a measure of disorder in the carbon materials and is inversely proportional to crystallite size, whereas the D4 band may be related to the presence of partially hydrogenated carbon elements in the disordered phase or on polygranular boundaries.

The I_D/I_G ratio for ECNFV is lower (2.69) as compared to as-received nanofibers (4.69) indicating a higher fraction of the better ordered carbon phase in the structure of these nanofibers (Table 3). It can be explained by a partial removing of the carbon phase more susceptible to oxidation

Table 4: Genotoxicity of samples after 1-hour and 24-hour incubation.

Samples	Control fibroblasts	ECNF	ECNFV
1 hour			
T-DNA	*3.45 ± 0.47* 2% dead cells	*8.35 ± 0.58* 22% dead cells	*3.81 ± 0.22* 6% dead cells
Student *t* vs. control	—	0.01	0.67
24 hours			
T-DNA	*3.90 ± 0.40* 4% dead cells	*11.19 ± 1.48* 24% dead cells	*5.12 ± 0.44* 4% dead cells
Student *t* vs. control	—	0.02	0.56

Table 5: Genotoxicity of samples after 1-hour and 24-hour incubation and after 1 Gy dose of X-ray irradiation.

Samples	Control fibroblasts	ECNF	ECNFV
1 hour			
T-DNA	*4.35 ± 0.73* 10% dead cells	*11.04 ± 0.29* 22% dead cells	*5.55 ± 0.68* 10% dead cells
Student *t* vs. control	—	0.03	0.34
24 hours			
T-DNA	*3.99 ± 0.70* 7% dead cells	*9.27 ± 0.87* 22% dead cells	*6.08 ± 0.91* 13% dead cells
Student *t* vs. control	—	0.01	0.23

during vacuum pressure treatment. Moreover, the crystallite size, L_a, is distinctly higher than that found in the as-received carbon nanofibers. It should be noted, however, that commercial PAN-based carbon fibers are characterized by an R_1 value less than 0.5 [52]. This indicates that the nanofibers tested in this study are characterized by a very low crystallinity, which may result from the nature of the polymer precursor and relatively low temperature of carbonization.

The spectra of the nanofibers also show second-order Raman peaks, known as the 2D bands, in the range from about 2500 cm^{-1} to 3100 cm^{-1} which can be used to characterize the structure of carbon materials and their susceptibility to graphitization (Figure 7). For less ordered carbon structures, the Raman spectrum shows a single 2D symmetric peak. The spectra in Figure 7 show broad overlapping symmetric peaks centered around 2694.3 cm^{-1} and 2689.6 cm^{-1} for ECNF and ECNFV, respectively. A small shift of peak towards a lower wavenumber value for ECNFV may result from the removal of the less-ordered carbon phase in the near-surface areas of this nanofiber. Raman spectra of both carbon nanofibers indicate that their structures contain various carbon components differing in crystalline degree. The air-treated nanofibers are characterized by a decrease in the average intensity ratio, I_D/I_G, in comparison to as-received nanofibers. This indicates that such a treatment caused some changes in the crystallinity of carbon nanofibers; i.e., the ratio between amorphous and crystalline components is changed, which is accompanied by shifting the average G-line positions to lower frequency and an increase in its intensity.

3.2. Biological Tests of Carbon Nanofibers. Genotoxicity of the carbon nanofibers was assessed by means of the comet test, in terms of the tail DNA, and the results are collected in Tables 4 and 5.

Results obtained for fibroblasts treated for 1 h with ECNF, without and with X-ray exposure, showed a significantly higher level of DNA damage for both nonirradiated ($p < 0.01$) and irradiated ($p < 0.03$) cells in comparison to untreated cells (Tables 4 and 5). Moreover, the presence of ECNF in culture medium caused an increase in the number of dead cells to 24%. On the contrary, in the ECNFV pretreated fibroblasts before and after 1 Gy dose of X-rays, the amount of DNA damage and the number of dead cells were similar to control. Impact assessment of nanomaterials for DNA repair on the basis of the DNA damage level in cells after 1 Gy and 24-hour incubation showed a significantly higher level for ECNF-pretreated fibroblasts ($p < 0.01$) in comparison to chemical untreated cells. The obtained results suggested that ECNF is a genotoxic material as evidenced by both the value of the T-DNA parameter indicating the increase in DNA strand damage and the number of dead cells observed in all experiments, while the second of the materials studied is not genotoxic, and statistical analysis indicates no statistically significant differences between the control and ECNFV. The ECNFV nanofibers introduced into the cell culture do not affect the repair processes in the cells contacting them.

Microphotographs of MG63 cell morphologies in contact with two types of carbon nanofibers and control sample are shown in Figure 8.

Analyzing the morphology of MG63 cells in contact with the nanofibers' significant differences in their behavior depending on the type of nanofibers can be observed. In case of the ECNF (Figure 8(b)), the cells were round and nonflattened, and many dead cells could be observed.

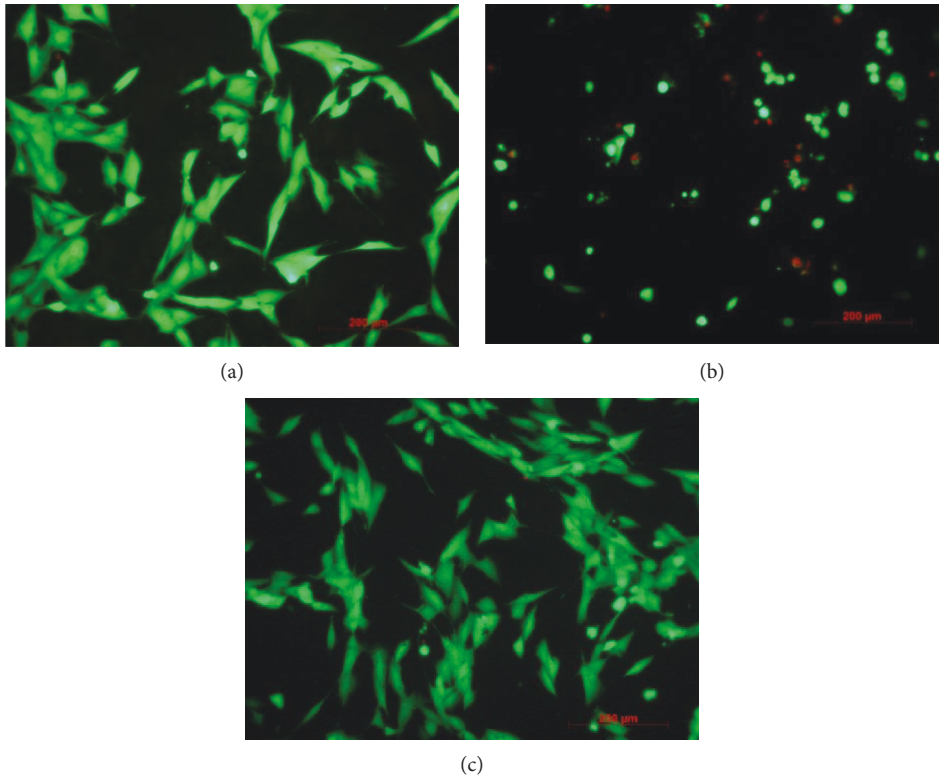

Figure 8: Fluorescence staining of MG 63 cells using calcein AM (green cells, viable cells) and propidium iodide (red cells, dead cells) after 24 h incubation in contact with the control sample (PS culture dish) (a), ECNF (b), and ECNFV (c).

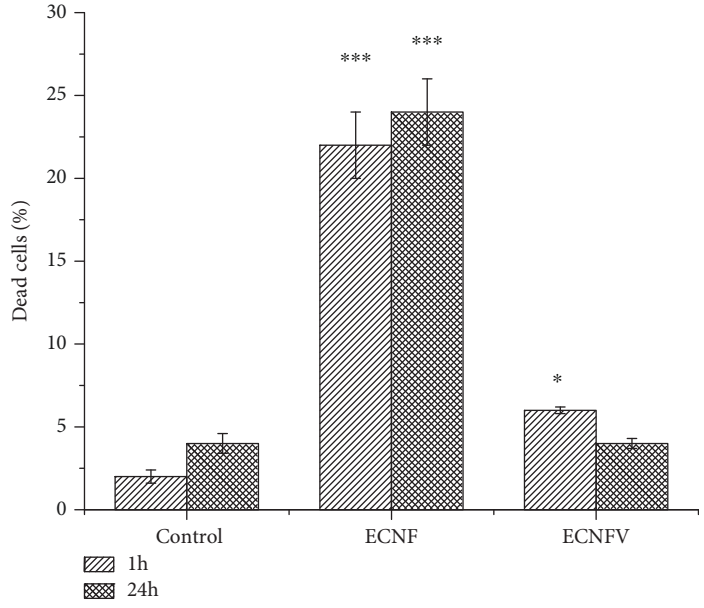

Figure 9: Number of dead fibroblast cells in contact with control, ECNF, and ECNFV samples. *Statistically significant ECNFV vs. control after 1 h incubation ($p < 0.05$). ***Statistically significant ECNF vs. control after 1 h and 24 incubation ($p < 0.01$).

On the contrary, cells that contacted with the ECNFV nanofibers (Figure 8(c)) were much better adhering to the substrate, they were well spread, and their shapes were similar to those found in the control (Figure 8(a)). No dead cells in contact with ECNFV were observed, which may indicate the lack of their cytotoxic effect. These results are consistent with the data obtained from the biological test of carbon mats in contact with fibroblasts (Figure 9).

The results of a nanofiber study in contact with both osteoblast-like cells and fibroblasts indicate the negative

effect of ECNF nanofibers on the cellular response, suggesting a certain cytotoxic effect of this material in the studied period of time.

The study showed that carbon nanofibers after the carbonization process have unfavorable characteristics as a biomaterial for biological use. Although carbon samples in the form of nanofibrous mat perform many advantageous properties for medical use including conductible structures for tissue engineering, the as-received samples assessed in genotoxicity and cytotoxicity tests behaved like toxic materials. Oxidation in the air is a simple way of modifying the biological properties of carbon nanofibers without deteriorating other physical and chemical properties important for use in medicine. Under the controlled surface treatment in air of nanofibers, significant changes in their surface morphology were observed. Raman spectroscopy has shown that the carbon structure is composed of several phases that vary in the degree of crystallinity. Raman spectra revealed that due to surface modification, the intensity of the (D) band associated with the less ordered carbon phase decreased, which resulted from the greater susceptibility of this phase to oxidation. For this reason, in the ECNFV sample the intensity of the G band increased. It is also worth mentioning that the surfaces of these nanofibers (Figure 1) were built with the separated polycrystalline carbon grains with rounded edges. The average size of these grains, depicted in the SEM images, was about 70 nm, while the values of L_a of crystallites determined from the Raman spectrum for ECNFV amounted to 7.1 nm (Table 3). It indicates that the separated carbon grains on the oxidized nanofibers' surface were composed of small carbon crystallites, whereas within the grain itself the crystallites joined together boundaries of a different structure than the boundaries between the polycrystalline grains forming the nanofibers (Table 2). Genotoxicity and cytotoxicity tests showed that such nanofibers behaved like a nontoxic material, in contrast to the as-received carbon nanofibers, which were found to be genotoxic and cytotoxic. The explanation of differences in the behavior of both carbon mats may be related to the nanotopography of their surfaces and difference in their structures. For biological tests, the mats were preliminarily disintegrated. Carbon nanofiber is made of crystallites of various structural ordering joined by intercrystallite boundaries in which carbon atoms form aliphatic and aromatic structures containing nitrogen, oxygen, and hydrogen. In the oxidation process, the carbon mat loses up to 8 wt% of the initial weight. During this process, the carbon phase more susceptible to oxidation is removed, i.e., carbon from intercrystallite boundaries and less ordered carbon fraction, e.g., carbon phase 3 identified by XRD analysis in ECNF. Removing a fraction of carbon from the carbon nanofiber changes the surface structure and shape of the carbon particles prepared for biological tests. We hypothesize that disintegrated carbon particles (nonoxidized) in contact with the cellular medium (also in comet assay) release aromatic and aliphatic carbon compounds, probably deriving from less ordered carbon phases including intercrystallite boundaries. Such compounds may be cytotoxic and genotoxic to a cellular response. However, such a hypothesis requires further research. Biological properties of carbon nanomaterials are a complex issue, in literature described inconsistently and ambiguously. It is well known that in the case of carbon nanoforms, especially those obtained in CVD processes with a well-defined structure, the factors influencing the cellular response in terms of cytotoxicity and genotoxicity are their size and shape, chemical state of the surface, and presence of the surface reactive oxygen species (ROS) that can damage DNA of cells [36]. On the other hand, carbon nanomaterials obtained by the carbonization of the electrospun polymer precursors are a different issue. In this case, the influence of all the above mentioned factors on the nature of the cellular response cannot be ruled out, though the carbonization products that may be toxic and genotoxic in contact with cells are of key importance.

The surface properties of carbon mats were studied by measuring the water contact angle. As is apparent from Table 1, the as–received carbon mat was hydrophobic (113.3°), and after oxidative treatment the mat became more hydrophilic (86.2°). Generally, hydrophilicity of a surface material designed, e.g., for scaffolds, is a favorable factor for regeneration of some types of tissues. Therefore, it appears that mats consisted of carbon nanofibers after the applied oxidation treatment have more favorable surface properties as potential substrates for tissue regeneration as compared to ECNF.

The applied oxidation treatment caused a slight increase in the resistivity of nanofibers, but they were still conductive materials. In addition, their microstructural parameters (porosity, nanofiber diameter) in the form of mats exhibited similar parameters as carbon mats prior to the oxidative modification. Thus, nontoxic oxidized mats can be the subject of further study for applications as electrode elements for electrical stimulation, as well as substrate elements of electrically activated cell cultures.

4. Conclusions

Carbon nanofibers in the form of mats were obtained from the electrospun PAN nanofiber precursor. The stabilized PAN nanofibers were carbonized up to 1000°C (ECNF) and additionally oxidized in air at 800°C under vacuum pressure (ECNFV). The final oxidized treatment enabled to decrease contact angles to provide a more hydrophilic character of the nanofibers' surface. The treatment in air under reduced pressure significantly changed the surface morphology of ECNFV and decreased the carbon phase fraction containing disordered carbon crystallites. A genotoxicity study of both types of carbon nanofibers showed differences in comet assay tests. The T-DNA test revealed that the surface-oxidized carbon nanofibers were not genotoxic, whereas the as-received carbon nanofibers indicated the increase in DNA strand damage and the number of dead cells as compared to control. ECNFV introduced into the cell culture did not affect the repair processes in the cells contacting them. The results demonstrated the enhancement in biocompatibility of the surface-oxidized carbon nanofibers determined by the T-DNA tests. Due to the removal of a part of carbon phase from the near-surface region, the carbon nanofibers with the specific surface nanotopography were manufactured. Such

nanofibers, thanks to their conductive properties, specific surface nanostructure, and biocompatibility, may be considered as promising substrates for electrical field stimulation regulating the behaviors of cells and as fibrous scaffolds for cell cultures. However, an assessment of the biological behavior of such a nanofiber requires further research on their biocompatibility including *in vitro* and *in vivo* tests, in longer periods of time.

Data Availability

The methods used to characterize the physical, chemical, structural, and biological properties of the samples and resulting data in the form of tables, figures, and images used to support the findings of this study are included within the article.

Conflicts of Interest

The authors declare that there is no conflict of interest regarding the publication of this paper.

Acknowledgments

This work has been supported by the Polish National Science Center, project no: 2017/25/B/ST8/02602, and by the Laryngology Department, School of Medicine, Medical University of Silesia in Katowice (Statute Found no.: KNW-1-102/K/8/0 and no.: KNW-1-043/K/7/0).

References

[1] T. J. Webster, Ed., *Nanomedicine: Technologies and Applications*, Woodhead Publishing, Oxford, PA, USA, 2012.

[2] Y. Nishimura, J. Ishii, C. Ogino, and A. Kondo, "Genetic engineering of bio-nanoparticles for drug delivery: a review," *Journal of Biomedical Nanotechnology*, vol. 10, no. 9, pp. 2063–2085, 2014.

[3] Y.-Y. Huang, S. K. Sharma, R. Yin, T. Agrawal, L. Y. Chiang, and M. R. Hamblin, "Functionalized fullerenes in photodynamic therapy," *Journal of Biomedical Nanotechnology*, vol. 10, no. 9, pp. 1918–1936, 2014.

[4] B. C. Janegitz, J. Cancino, and V. Zucolotto, "Disposable biosensors for clinical diagnosis," *Journal of Nanoscience and Nanotechnology*, vol. 14, no. 1, pp. 378–389, 2014.

[5] L. Zhang and T. J. Webster, "Nanotechnology and nanomaterials: promises for improved tissue regeneration," *Nano Today*, vol. 4, no. 1, pp. 66–80, 2009.

[6] K. R. Chien, "Regenerative medicine and human models of human disease," *Nature*, vol. 453, no. 7193, pp. 302–305, 2008.

[7] F. J. O'Brien, "Biomaterials & scaffolds for tissue engineering," *Materials Today*, vol. 14, no. 3, pp. 88–95, 2011.

[8] R. Balint, N. J. Cassidy, and S. H. Cartmell, "Electrical stimulation: a novel tool for tissue engineering," *Tissue Engineering Part B: Reviews*, vol. 19, no. 1, pp. 48–57, 2013.

[9] G. Shi, Z. Zhang, and M. Rouabhia, "The regulation of cell functions electrically using biodegradable polypyrrole–polylactide conductors," *Biomaterials*, vol. 29, no. 28, pp. 3792–3798, 2008.

[10] R. Huo, Q. Ma, J. J. Wu et al., "Noninvasive electromagnetic fields on keratinocyte growth and migration," *The Journal of Surgical Research*, vol. 162, no. 2, pp. 299–307, 2010.

[11] M. Zhao, "Electrical fields in wound healing—an overriding signal that directs cell migration," *Seminars in Cell & Developmental Biology*, vol. 20, no. 6, pp. 674–682, 2009.

[12] M. Radisic, H. Park, H. Shing et al., "Functional assembly of engineered myocardium by electrical stimulation of cardiac myocytes cultured on scaffolds," *Proceedings of the National Academy of Sciences of the United States of America*, vol. 101, no. 52, pp. 18129–18134, 2004.

[13] W. Zhu, T. Ye, S.-J. Lee et al., "Enhanced neural stem cell functions in conductive annealed carbon nanofibrous scaffolds with electrical stimulation," *Nanomedicine: Nanotechnology, Biology and Medicine*, vol. 14, no. 7, pp. 2485–2494, 2018.

[14] C. P. Huang, X. M. Chen, and Z. Q. Chen, "Osteocyte: the impresario in the electrical stimulation for bone fracture healing," *Medical Hypotheses*, vol. 70, no. 2, pp. 287–290, 2008.

[15] L. Li, Y. H. El-Hayek, B. Liu et al., "Direct-current electrical field guides neuronal stem/progenitor cell migration," *Stem Cells*, vol. 26, no. 8, pp. 2193–2200, 2008.

[16] S. Mobini, L. Leppik, V. Thottakkattumana Parameswaran, and J. H. Barker, "*In vitro* effect of direct current electrical stimulation on rat mesenchymal stem cells," *PeerJ*, vol. 5, article e2821, 2017.

[17] A. S. Rowlands and J. J. Cooper-White, "Directing phenotype of vascular smooth muscle cells using electrically stimulated conducting polymer," *Biomaterials*, vol. 29, no. 34, pp. 4510–4520, 2008.

[18] B. Ercan and T. J. Webster, "The effect of biphasic electrical stimulation on osteoblast function at anodized nanotubular titanium surfaces," *Biomaterials*, vol. 31, no. 13, pp. 3684–3693, 2010.

[19] J. Ringe, C. Kaps, G.-R. Burmester, and M. Sittinger, "Stem cells for regenerative medicine: advances in the engineering of tissues and organs," *Die Naturwissenschaften*, vol. 89, no. 8, pp. 338–351, 2002.

[20] B. Zhu, M. Nicholls, Y. Gu et al., "Electric signals regulate the directional migration of oligodendrocyte progenitor cells (OPCs) via β1 integrin," *International Journal of Molecular Sciences*, vol. 17, no. 11, p. 1948, 2016.

[21] Z. Dong, Z. Pei, Z. Li, Y. Wang, A. Khan, and X. Meng, "Electric field stimulation induced neuronal differentiation of filum terminale derived neural progenitor cells," *Neuroscience Letters*, vol. 651, pp. 109–115, 2017.

[22] T. Stöver and T. Lenarz, "Biomaterials in cochlear implants," *GMS Current Topics in Otorhinolaryngology - Head and Neck Surgery*, vol. 8, article Doc10, 2009.

[23] F.-G. Zeng, S. J. Rebscher, Q.-J. Fu et al., "Development and evaluation of the Nurotron 26-electrode cochlear implant system," *Hearing Research*, vol. 322, pp. 188–199, 2015.

[24] Y. S. Lim, S.-I. Park, Y. H. Kim, S. H. Oh, and S. J. Kim, "Three-dimensional analysis of electrode behavior in a human cochlear model," *Medical Engineering & Physics*, vol. 27, no. 8, pp. 695–703, 2005.

[25] Z. Hu and M. Ulfendahl, "Cell replacement therapy in the inner ear," *Stem Cells and Development*, vol. 15, no. 3, pp. 449–459, 2006.

[26] E. Bas, T. R. Van De Water, V. Lumbreras et al., "Adult human nasal mesenchymal-like stem cells restore cochlear spiral

ganglion neurons after experimental lesion," *Stem Cells and Development*, vol. 23, no. 5, pp. 502–514, 2014.

[27] M. N. Rivolta, "Developing a stem cell-based therapy for the treatment of hearing loss," *Hearing, Balance and Communication*, vol. 13, no. 4, pp. 148–152, 2015.

[28] H. Kasagi, T. Kuhara, H. Okada, N. Sueyoshi, and H. Kurihara, "Mesenchymal stem cell transplantation to the mouse cochlea as a treatment for childhood sensorineural hearing loss," *International Journal of Pediatric Otorhinolaryngology*, vol. 77, no. 6, pp. 936–942, 2013.

[29] P. A. Tran, L. Zhang, and T. J. Webster, "Carbon nanofibers and carbon nanotubes in regenerative medicine," *Advanced Drug Delivery Reviews*, vol. 61, no. 12, pp. 1097–1114, 2009.

[30] J. Venkatesan, R. Pallela, and S.-K. Kim, "Applications of carbon nanomaterials in bone tissue engineering," *Journal of Biomedical Nanotechnology*, vol. 10, no. 10, pp. 3105–3123, 2014.

[31] A. Fraczek-Szczypta, "Carbon nanomaterials for nerve tissue stimulation and regeneration," *Materials Science and Engineering: C*, vol. 34, pp. 35–49, 2014.

[32] A. Fraczek-Szczypta, E. Menaszek, T. B. Syeda et al., "Effect of MWCNT surface and chemical modification on in vitro cellular response," *Journal of Nanoparticle Research*, vol. 14, no. 10, article 1181, 2012.

[33] E. Ben-Jacob and Y. Hanein, "Carbon nanotube microelectrodes for neuronal interfacing," *Journal of Materials Chemistry*, vol. 18, no. 43, p. 5181, 2008.

[34] J. V. Veetil and K. Ye, "Tailored carbon nanotubes for tissue engineering applications," *Biotechnology Progress*, vol. 25, no. 3, pp. 709–721, 2009.

[35] C.-W. Lam, J. T. James, R. McCluskey, S. Arepalli, and R. L. Hunter, "A review of carbon nanotube toxicity and assessment of potential occupational and environmental health risks," *Critical Reviews in Toxicology*, vol. 36, no. 3, pp. 189–217, 2006.

[36] A. A. Shvedova, E. R. Kisin, D. Porter et al., "Mechanisms of pulmonary toxicity and medical applications of carbon nanotubes: two faces of Janus?," *Pharmacology & Therapeutics*, vol. 121, no. 2, pp. 192–204, 2009.

[37] L. M. Sargent, S. H. Reynolds, and V. Castranova, "Potential pulmonary effects of engineered carbon nanotubes: *in vitro* genotoxic effects," *Nanotoxicology*, vol. 4, no. 4, pp. 396–408, 2010.

[38] A. Fraczek, E. Menaszek, C. Paluszkiewicz, and M. Blazewicz, "Comparative in vivo biocompatibility study of single- and multi-wall carbon nanotubes," *Acta Biomaterialia*, vol. 4, no. 6, pp. 1593–1602, 2008.

[39] S. Vardharajula, S. Z. Ali, P. M. Tiwari et al., "Functionalized carbon nanotubes: biomedical applications," *International Journal of Nanomedicine*, vol. 7, pp. 5361–5374, 2012.

[40] M. Allegri, D. K. Perivoliotis, M. G. Bianchi et al., "Toxicity determinants of multi-walled carbon nanotubes: The relationship between functionalization and agglomeration," *Toxicology Reports*, vol. 3, pp. 230–243, 2016.

[41] S. L. Montes-Fonseca, E. Orrantia-Borunda, A. Aguilar-Elguezabal, C. González Horta, P. Talamás-Rohana, and B. Sánchez-Ramírez, "Cytotoxicity of functionalized carbon nanotubes in J774A macrophages," *Nanomedicine: Nanotechnology, Biology and Medicine*, vol. 8, no. 6, pp. 853–859, 2012.

[42] L. Zhou, H. J. Forman, Y. Ge, and J. Lunec, "Multi-walled carbon nanotubes: a cytotoxicity study in relation to functionalization, dose and dispersion," *Toxicology In Vitro*, vol. 42, pp. 292–298, 2017.

[43] L. Zhang, J. Xia, Q. Zhao, L. Liu, and Z. Zhang, "Functional graphene oxide as a nanocarrier for controlled loading and targeted delivery of mixed anticancer drugs," *Small*, vol. 6, no. 4, pp. 537–544, 2010.

[44] X. Sun, Z. Liu, K. Welsher et al., "Nano-graphene oxide for cellular imaging and drug delivery," *Nano Research*, vol. 1, no. 3, pp. 203–212, 2008.

[45] M. C. Serrano, J. Patiño, C. García-Rama et al., "3D free-standing porous scaffolds made of graphene oxide as substrates for neural cell growth," *Journal of Materials Chemistry B*, vol. 2, no. 34, p. 5698, 2014.

[46] N. Li, Q. Zhang, S. Gao et al., "Three-dimensional graphene foam as a biocompatible and conductive scaffold for neural stem cells," *Scientific Reports*, vol. 3, no. 1, 2013.

[47] Q. Tu, L. Pang, Y. Chen et al., "Effects of surface charges of graphene oxide on neuronal outgrowth and branching," *Analyst*, vol. 139, no. 1, pp. 105–115, 2014.

[48] L. Zhang, A. Aboagye, A. Kelkar, C. Lai, and H. Fong, "A review: carbon nanofibers from electrospun polyacrylonitrile and their applications," *Journal of Materials Science*, vol. 49, no. 2, pp. 463–480, 2014.

[49] S. K. Nataraj, K. S. Yang, and T. M. Aminabhavi, "Polyacrylonitrile-based nanofibers—a state-of-the-art review," *Progress in Polymer Science*, vol. 37, no. 3, pp. 487–513, 2012.

[50] Z. Zhou, C. Lai, L. Zhang et al., "Development of carbon nanofibers from aligned electrospun polyacrylonitrile nanofiber bundles and characterization of their microstructural, electrical, and mechanical properties," *Polymer*, vol. 50, no. 13, pp. 2999–3006, 2009.

[51] A. Panek, A. Fraczek-Szczypta, E. Dlugon, M. Nocun, C. Paluszkiewicz, and M. Blazewicz, "Genotoxicity study of carbon nanoforms using a comet assay," *Acta Physica Polonica A*, vol. 133, no. 2, pp. 306–308, 2018.

[52] P. Musiol, P. Szatkowski, M. Gubernat, A. Weselucha-Birczynska, and S. Blazewicz, "Comparative study of the structure and microstructure of PAN-based nano- and micro-carbon fibers," *Ceramics International*, vol. 42, no. 10, pp. 11603–11610, 2016.

[53] M. Wojdyr, "Fityk: a general-purpose peak fitting program," *Journal of Applied Crystallography*, vol. 43, no. 5, pp. 1126–1128, 2010.

[54] S. Costa, E. Borowiak-Palen, M. Kruszynska, A. Bachmatiuk, and R. J. Kalenczuk, "Characterization of carbon nanotubes by Raman spectroscopy," *Materials Science-Poland*, vol. 26, pp. 433–441, 2008.

[55] N. Takeda and K. Murakoshi, "Characteristics of the Raman spectra of single-walled carbon nanotube bundles under electrochemical potential control," *Analytical and Bioanalytical Chemistry*, vol. 388, no. 1, pp. 103–108, 2007.

[56] A. Cebulska-Wasilewska, A. Panek, Z. Żabiński, P. Moszczyński, and W. W. Au, "Occupational exposure to mercury vapour on genotoxicity and DNA repair," *Mutation Research/Genetic Toxicology and Environmental Mutagenesis*, vol. 586, no. 2, pp. 102–114, 2005.

[57] A. Cebulska-Wasilewska, I. Pawłyk, A. Panek et al., "Exposure to environmental polycyclic aromatic hydrocarbons: influences on cellular susceptibility to DNA damage (sampling Košice and Sofia)," *Mutation Research/Fundamental and*

Molecular Mechanisms of Mutagenesis, vol. 620, no. 1-2, pp. 145–154, 2007.

[58] M. W. Smith, I. Dallmeyer, T. J. Johnson et al., "Structural analysis of char by Raman spectroscopy: improving band assignments through computational calculations from first principles," *Carbon*, vol. 100, pp. 678–692, 2016.

[59] F. Tuinstra and J. L. Koenig, "Raman spectrum of graphite," *The Journal of Chemical Physics*, vol. 53, no. 3, pp. 1126–1130, 1970.